ACS APPLIED MATERIALS & INTERFACES

RESEARCH ARTICLE

www.acsami.org

$Co_{1-x}Mg_xMoO_4$ Compounds for Pressure Indicators

L. Righetti,[†] L. Robertson,[†] A. Largeteau,[†] G. Vignoles,[‡] A. Demourgues,[†] and M. Gaudon*[,†]

[†]CNRS, Université de Bordeaux, ICMCB, 87 avenue du Dr. Albert Schweitzer, F-33608 Pessac Cedex (France),

[‡]University Bordeaux, Laboratoire des Composites ThermoStructuraux (LCTS), UMR 5801: CNRS-Safran-CEA-UB1, Domaine Universitaire de Bordeaux, 3, Allée de La Boétie, 33600 Pessac (France)

ABSTRACT: Two $Co_{1-x}Mg_xMoO_4$ oxide compositions ($x = 0$ and $x = 0.4$) were investigated as potential pressure indicators. The first order phase half-transition induced by pressure application from the β to the α form, i.e. from the high temperature/low pressure form to the high pressure/low temperature form, was studied thanks to the powder diffuse reflection (color) evolution versus the applied pressure. Three key parameters were analyzed: (i) the magnesium content, (ii) the powder grain sizes, (iii) the pressure application mode (uniaxial or isostatical). It was shown these three parameters allow tuning the transition pressure in a wide range from few bars to few kbars.

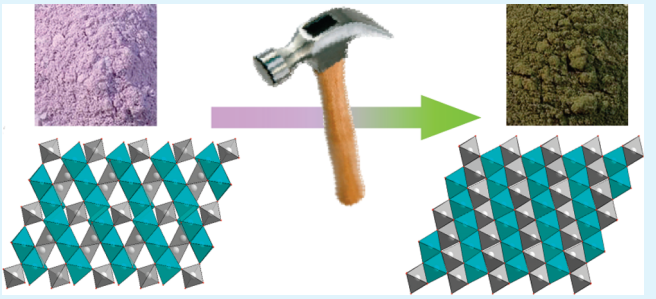

KEYWORDS: phase transition, piezochromism, pressure indicators, color, pigments, molybdates

1. INTRODUCTION

Piezochromic oxides are able to mark pressure or constrain by a drastic color change. The piezochromic oxides, for which an irreversible phase transition is induced by a pressure, are very rare. The Boolean research on the associated terms (oxides + piezochromic) led only to three occurences,[1−3] two of them concerning $AMoO_4$ molybdates.[2,3] On the basis of our previous studies on the $CuMoO_4$ molybdates family,[4−9] which has shown piezochromic possibilities, various members of the $Co_{1-x}Mg_xMoO_4$ series that crystallize in the α $CoMoO_4$ and/or β $CoMoO_4$ structure-types with $C2/m$ space group were herein studied. In the α form, both Co^{2+} and Mo^{6+} ions occupy distorted octahedral sites. In the β form, Co^{2+} ions remain in distorted octahedral sites, whereas Mo^{6+} is 4-fold coordinated to oxygen in distorted tetrahedral sites.[10−13] The occurrence of a total $Co_{1-x}Mg_xMoO_4$ solid solution was demonstrated in one of our previous studies,[14] dealing with the study of the thermochromic phenomenon of the $Co_{1-x}Mg_xMoO_4$ solid solution, from the accurate analysis of the XRD patterns (peak positions and intensities). The presence of this solid-solution represents a strong advantage besides the $CuMoO_4$ oxides family for which the concentrations of Cu^{2+} or Mo^{6+} ions substituting cations (W^{6+}, Mg^{2+}, Co^{2+}, Zn^{2+}...) preserving the $CuMoO_4$ structure-type are very low.[4,5] The first order transition between both (Co, Mg)MoO_4 allotropic forms occur at temperature ranging from about 300 to 500 °C depending on the magnesium rate, with an hysteresis width between the $\alpha \rightarrow \beta$ and the $\beta \rightarrow \alpha$ transitions at about 400 °C. The $\alpha \rightarrow \beta$ half-transition is accompanied by a cell volume expansion of 6%. Both α-from and β-form spectra show two optical contributions to the color in the $Co_{1-x}Mg_xMoO_4$ compounds: typical d−d Co^{2+} ions transitions in an octahedral site and a high energy $O^{2-} \rightarrow Mo^{6+}$ charge transfer. This charge transfer gap strongly shifts from 2.4 eV (green range) for the α-form to 2.9 eV for the β-one (UV−visible frontier) consecutively to the change of molybdenum coordination. This gap shift is at the origin of the significant color change of the compound. The violet color of the β−$CoMoO_4$ form, where the $O^{2-} \rightarrow Mo^{6+}$ charge transfer is located at the UV−visible frontier, is therefore mainly caused by the Co^{2+} ions absorption bands: three d-d Co^{2+} bands: $^4T_{1g} \rightarrow {}^4T_{2g}(F)$, $^4T_{1g} \rightarrow {}^4A_{2g}(F)$, $^4T_{1g} \rightarrow {}^4T_{1g}(P)$ with the third one (the most intense) centered on yellow wavelengths (about 500−600 nm).[15,16] The spectra were recorded on the two allotropic forms, for the extreme $CoMoO_4$ composition (Figure 1). The dark green color of the α form is due to the convolution of the same Co^{2+} d−d bands plus the $O^{2-} \rightarrow Mo^{6+}$ charge transfer, which is here responsible for an additional absorption of the violet and blue wavelengths.

In the present study, the focus was made on the $\beta \rightarrow \alpha$ half-transition induced via applied pressure. Two different pressure application modes were tested and compared: an isostatic pressure mode via the pressurization of a fluid media and a uniaxial pressure mode perfomed on powder pellets. For both pressure application modes, the effects of the powder grain sizes and magnesium content were measured and discussed.

2. EXPERIMENTAL SECTION

2.1. Synthesis. $Co_{1-x}Mg_xMoO_4$ powders with β-form were prepared by solid-state reaction from stoichiometric amounts of MoO_3

Received: January 28, 2011
Accepted: March 16, 2011
Published: March 16, 2011

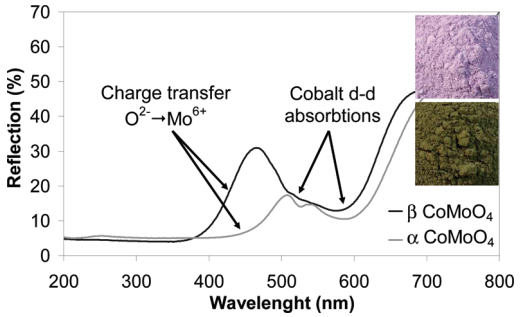

Figure 1. Reflectivity (%) spectra for α and β-$CoMoO_4$ powders with photographs in inset.

(Sigma 99.5%), Co_3O_4 (Alfa Aesar 99.7%) and MgO (Cerac Pure 99.95%). Mixture of the reactants was heated in an alumina crucible at 700 °C for 20 h and slowly cooled to room temperature, leading to the pure β form (low pressure/high temperature form).

2.2. Powder X-ray Diffraction. Powder X-ray diffraction patterns were recorded on a Philips PW 1820 apparatus equipped with a $K\alpha_1$/$K\alpha_2$ source and a copper anticathode. Diffraction patterns were collected with a 2θ step of 0.02° with a counting time of 10 s per step in routine mode. X-ray powder diffraction was used in order to check that all the synthesized (Mg−Co)MoO_4 solid solutions are pure. For crystallite size calculation with Debye−Scherrer model, proper standard spectra for defining the apparatus broadening are recorded; this instrumental contribution is then subtracted to the X-ray signal in order to obtain the sample contribution only.

2.3. Reflectivity Measurements. Visible−NIR spectroscopic analyses were carried out in Diffuse Reflectance mode with a Konica-Minolta CM-700d spectrophotometer equipped with an integrating sphere coated with polytetrafluoroethylene. Measurements were performed for wavelengths varying from 200 up to 800 nm, in Specular Component Excluded (SCE) mode. A white calibration cap CM-A177 (ceramic) was used as white reference and the standard D65 (Daylight, color temperature: 6504K) with a 10° observer angle (CIE1964) as illuminant. Only the UV−visible wavelength range and the La^*b^* space parameters (L, luminosit; a^*, green to red axis; and b^*, yellow to blue axis coefficients) were considered. No computing mathematics treatment was performed since the apparatus directly sets La^*b^* chromatic parameters. The a^* colorimetric parameter is descriptive of the green-red hue axis. This parameter was chosen in order to quantify the α and β forms ratio inside powder sample during the phase transition since the a^* value is very different for the two allotropic forms: for $CoMoO_4$ composition, $a^* = -5.1$ and $+11.2$ for α and β-forms, respectively. The quantification of each phase was made considering a^* values respect a mixture law besides the β and α forms a^* values.

2.4. Pressure Application Processes. Pressure was applied using two different processes: (i) ultrahigh hydrostatic pressure was induced from oil media and (ii) uniaxial pressure was applied on powder pellets.

In the first process, the oxide powder was dispersed in ethanol; the obtained suspension was thermally sealed in a nonporous polyethylene bag (Cryovac-NOP-120). The hyperbar experimental apparatus was designed and produced by NFM-Technologies (Le Creusot, France) and Framatome (Paris, France) and marketed by CLEXTRAL (Firminy, France). The sample bags were hydrostatically pressed in a 3 L sample compartment at various pressures ranging from 500 to 6000 bar at ambient temperature and with a pressure-climbing rate of about 4000 bar per minute. Both pressure and temperature were permanently monitored and recorded during the process.

In the second process, the powder samples were introduced in a 8 mm pellet matrix in order to get in a reproducible way about 2 mm of pellet thickness after pressure application. The pressure was applied thanks to a home-built scalepan balance in which a counter mass was used in a lever system with a pivot point in order to multiply the mechanical force (effort) that can be applied on the piston of the pellet matrix. The balance hence represents a class 2 lever for which the load is situated between the pivot point and the force (Figure 2). In this mode, the engineering stress on the powder was defined as the ratio of the weight to the pellet diameter.

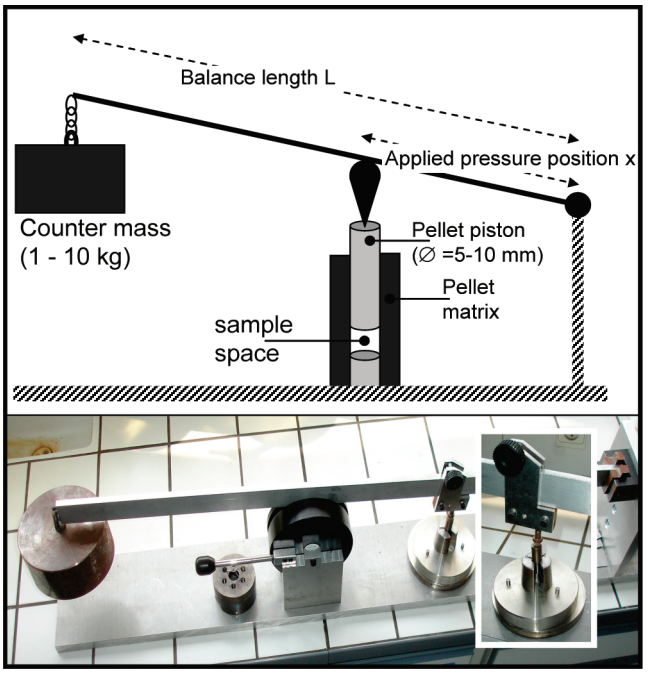

Figure 2. As-scalepan balance system used as the applied pressure apparatus in the uniaxial pressure mode.

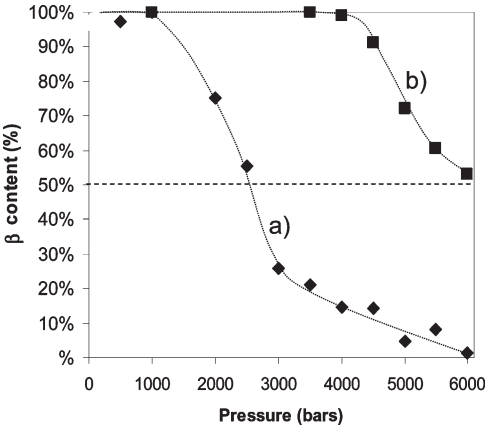

Figure 3. β-form content versus applied pressure using isostatic mode for (a) $CoMoO_4$ and (b) $Co_{0.6}Mg_{0.4}MoO_4$ compound.

3. RESULTS AND DISCUSSION

3.1. Isostatic Pressure Mode. In a first step, the influence of the Co/Mg ratio on the piezochromic transition pressure was studied. Hence, as shown in Figure 3, the β-form content progressively decreases with a sigmoid curve versus the applied

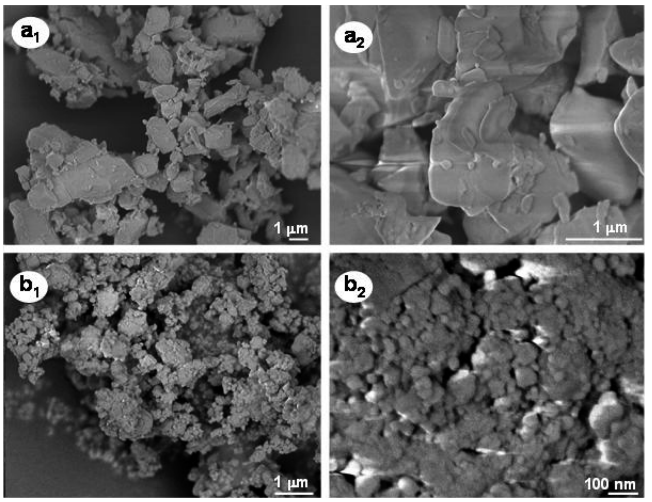

Figure 4. (a) SEM micrographs of the $CoMoO_4$ compound a) fresh oxide obtained after synthesis at 700 °C, (b) oxide obtained after mechanical grinding for 60 min (a1) and (b1) micrographs are obtained with small magnification, (a2) and (b2) with large magnification.

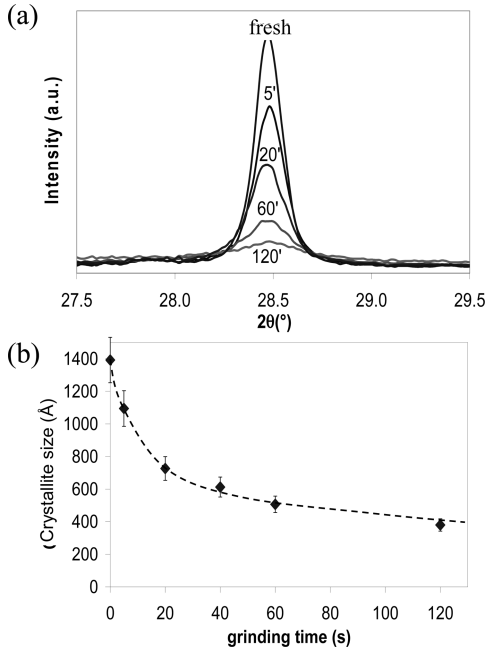

Figure 5. Evolution of the $CoMoO_4$ powder grain size versus grinding time. (a) Following of the evolution of one diffraction peak shape of the $CoMoO_4$ compound after various times of mechanical grinding. (b) Diminution of the powder grain size—peak width increase—versus grinding time; the calculation is issued from the Debye—Scherrer law applied to the X-ray powder patterns.

pressure. It has been already demonstrated on the $CuMo_{1-x}W_xO_4$ solid solution,[3] that the strong octahedral coordination preference of the tungsten ions leads to a decrease of the piezochromic transition pressure. Herein, the Mg^{2+} ions are more electropositive than the Co^{2+} ones. Hence, the $A^{2+}—O^{2-}$ bonds are more ionic in the $Co_{0.6}Mg_{0.4}MoO_4$ compound than in the $CoMoO_4$ one. From a competitive bond effect, the $Mo^{6+}—O^{2-}$ bonds then tends to become more covalent while

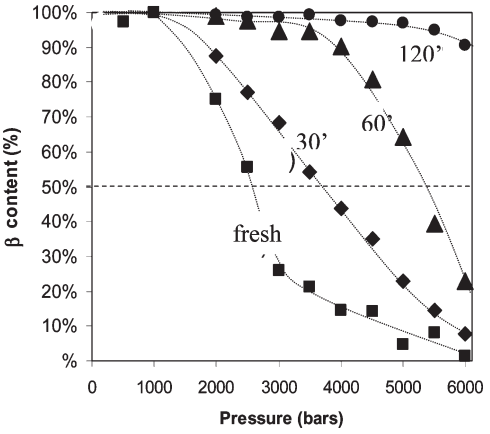

Figure 6. β-form content versus applied pressure using isostatic mode for fresh $CoMoO_4$ and $CoMoO_4$ obtained after grinding for 30, 60, and 120 min.

Mg^{2+} ions are inserted. Thus, the substitution of a part of Co^{2+} ions by Mg^{2+} ions stabilizes $Mo—O_4$ tetrahedral sites, i.e., the high-temperature/low-pressure violet form is relatively stabilized in comparison to the low-temperature/high-pressure green form. Comparing both compositions, the decrease of the low pressure form content in pressed samples versus applied pressure is more rapid for the $CoMoO_4$ powder than for the $Co_{0.6}Mg_{0.4}MoO_4$ compound. The P50 transition pressure — for which the samples contain 50 vol % of low and 50 vol % of high pressure form — are about 2500 bar and 6000 bar for $CoMoO_4$ and $Co_{0.6}Mg_{0.4}MoO_4$ compounds, respectively. Moreover, the low pressure form content curve versus pressure respects a S curve shape, with a smooth S second branch such as the transition spreads from 1500 to 6000 bar, i.e., with a total width at about 4500 bar for the $CoMoO_4$ compound.

In a second step, the study dealt with the influence of the grain size on the transition pressure. To vary the grain sizes, a mechanical grinding was performed, with the grinding time being the parameter of control. The grinding process induces a near-complete β to α phase transformation. Thus, in order to get again the pure β-form, a short additional annealing at 600 °C for 3 min was performed. This short annealing allows obtaining the pure β-phase without inducing the powder sintering (grain growth). This study was done on the $CoMoO_4$ reference composition. SEM micrographs of the fresh oxide and the 60 min ground oxide were compared (Figure 4). One can already see the efficiency of the mechanical grinding here employed. A zoom on one X-ray diffraction peak in order to illustrate the amorphization effect produced by the mechanical grinding is reported in Figure 5a. Obviously, the peak width becomes progressively larger versus grinding time. The Debye—Scherrer law—linking the peak width (fwhm: Full Width at Half-Maximum) to the crystallite diameter considering quasi-spherical particle shape—was used in order to propose the evolution of the powder crystallite size versus grinig time; this evolution is reported in Figure 5b. The crystallite size decrease leads to an increase of the transition pressure required for producing the piezochromic phase transformation. Figure 6 shows that the P50 transition pressures were shifted from 2500 bar for the fresh oxide to 4000, 5500, and largely over 6000 bar for the 30, 60, and 120 min ground oxides, respectively. Moreover, the transition becomes sharper, especially for the 60 min sample; this

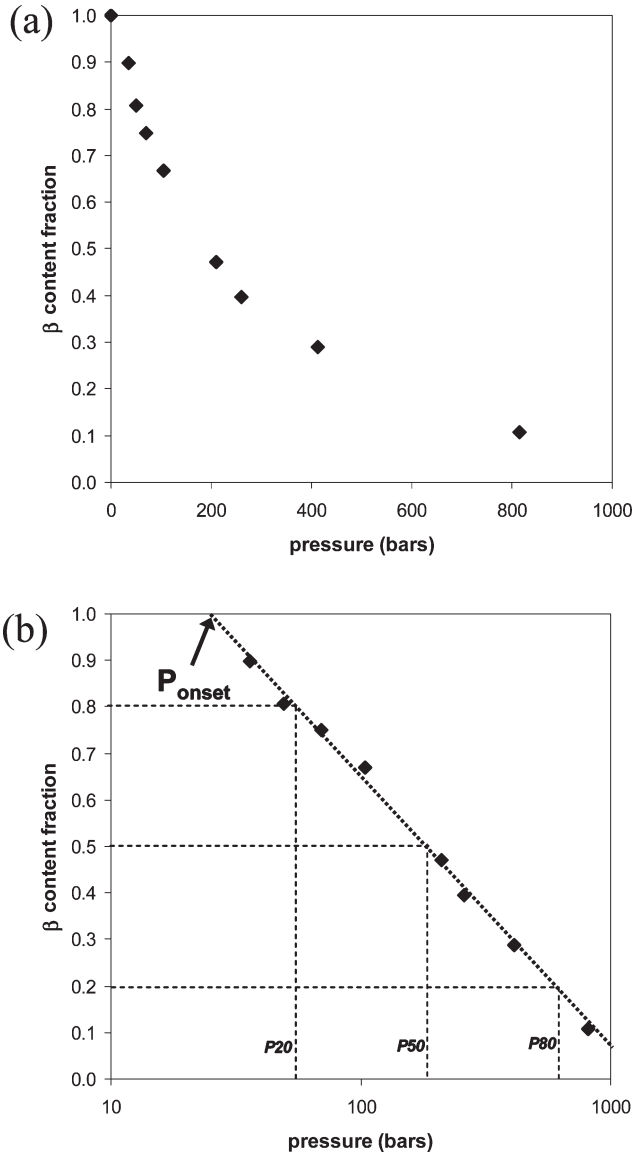

Figure 7. (a) β-form content versus applied pressure using uniaxial mode for the $CoMoO_4$ compound. (b) Illustration using logarythmic pressure scale.

phenomenon may be due to a sharper crystallite size distribution of the ground powder, the grinding being more efficient on the bigger crystallites. Our interpretation of the grain size influence is the grain surfaces stabilize low atomic coordination number, as was already reported on $CuMoO_4$.[5]

The piezochromic phase transition studied through the isostatic application mode allowed showing that the piezochromic transition pressures can be tuned not only from the raw oxide composition, i.e., atomic substitutions within solid solutions domain, but also from the grain morphology.

3.2. Uniaxial Pressure Mode. The uniaxial pressure mode study was performed in a similar way as in the isostatical mode; firtsly, the two same compositions ($CoMoO_4$ and $Co_{0.6}Mg_{0.4}MoO_4$ compounds) were compared and second, the influence of the crystallite size was studied thanks to the application of a grinding process during various grinding times performed on the $CoMoO_4$ reference compound.

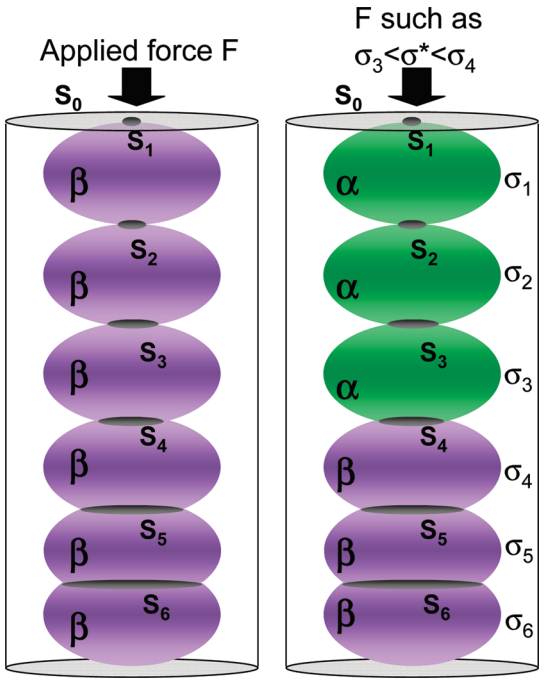

Figure 8. Scheme of the powder represented as a stacking of equal grains with distinct contact area sizes (transformation of the purple β-form into green α-form versus with applied constrain).

The P50 transition pressure measured in uniaxial mode are 1 order of magnitude lower than for the isostatic mode, 200 bar instead of 2000 bar for the CoMoO4 fresh oxide (Figures 7). One can note that the color of the pellet is homogeneous (no phase segregations at the surfaces are detected). The powder pellet can be seen as a "granular skeleton" made of successive layers of grains in contact each other by a "grains contact surface". Hence the real pressure transmitted to each grain is not equal to the pressure calculated as the applied strength normalized by the pellet surface. The small effective areas of contact between particles through which pressure is conducted inside the whole pellet is without any doubt at the origin of the strong shift observed between the two pressure application modes. Moreover, the shape of the low pressure form content versus pressure curve appears different. Indeed, the phase transformation advancement does not respect a S curve shape but an asymptotic decay (Figure 7a). Actually, the asymptotic decay occurs with roughly a logarithmic kinetic as the linear evolution of the phase transformation advancement versus the $\log(P)$, reported in Figure 7b, shows. The transition spread out represents one pressure decade and can not be only the consequence of the large crystallite size distribution. The material is built of a collection of grains, which were each susceptible to undergo a transformation as soon a part of any grain, with critical section S, suffered a stress which is superior to its transformation stress σ^*. The corresponding force is $F = \sigma^* S$. Let us call $\varphi(S)$ the volume fraction distribution of grains according to their critical sections. The granular skeleton under pressure can be thus represented as a column of grains (Figure 8). The following relationships between the amount of beta phase and $\varphi(S)$ can be proposed

$$\beta(S) = 1 - \int_{S_{min}}^{S} \varphi(S)dS \text{ and } d\beta = -\varphi(S)dS$$

Table 1. Results of the Statistical Analysis on the β-Form Content versus Applied Pressure

distribution	regression coefficient	parameters	mean and S.D.
exponential $\beta(P) = \exp(-(P/P_0))$	$\rho^2 = 0.996$	$P_0 = 34.4$ MPa	$\langle P\rangle = 34.4$ MPa
			s.d. = 34.4 MPa
piecewise linear of log $\beta(P) = 1 - K\ln(P/P_{min})$ if P $\in[P_{min}, P_{max}]$	$\rho^2 = 0.995$	$K = 0.2541$	$\langle P\rangle = 31.8$ MPa
		$P_{min} = 2.49$ MPa	s.d. = 45.5 MPa
		$P_{max} = 127.64$ MPa	
log-normal $\beta(P) = \Phi((\ln(P) - \mu)/\sigma)$	$\rho^2 = 0.997$	$\mu = 16.747$	$\langle P\rangle = 48.6$ MPa
		$\sigma = 1.38$	s.d. = 61.3 MPa
Weibull $\beta(P) = \exp(-(P/P_0)^m)$	$\rho^2 = 0.998$	$m = 0.83$	$\langle P\rangle = 33.5$ MPa
		$P_0 = 30.3$ MPa	s.d. = 41.8 MPa

Similarly, the amount of beta phase is distributed as a function of the applied force

$$\beta(F) = 1 - \sigma^{*-1}\int_{F_{min}}^{F}\varphi(F/\sigma^*)dF$$

The data are given in terms of the applied force F divided by the device section S_0, which will be noted as an engineering compressive stress R (corresponding to the pressure reported in previous figures)

$$\beta(R) = 1 - (S_0/\sigma^*)\int_{R_{min}}^{R}\varphi(RS_0/\sigma^*)dR$$

Or, more simply

$$\beta(R) = 1 - \int_{R_{min}}^{R}\psi(R)dR \text{ where}$$
$$\psi(R) = (S_0/\sigma^*)\varphi(RS_0/\sigma^*)$$

Three distributions have been fitted to the experimental results. Table 1 collects the results of the statistical analyses. The regression coefficients are satisfying for the three tested distributions. The agreement is excellent for the log-normal distribution, which is frequently found in the description of grain size distributions in powders. Indeed, it is expected that the distribution of the critical area S is closely related to the size distribution itself. The agreement is also excellent for a Weibull distribution. The Weibull exponent is close to 1 ($m = 0.83$), which indicates a rather large dispersion. The fit is slightly less satisfying for the ≪ piecewise linear of log ≫ distribution, in which it is seen that the probability density is inversely proportional to the applied force, i.e., to the critical section size S in a pressure interval: between P_{min} (or P_{onset}) and P_{max}. This fit corresponds to the linear decay of the phase transformation advancement versus the log(P), reported previously in dot line in Figure 7b. In contrast with the preceding distributions, this one is only defined on an interval of stresses; the value of the maximal compressive stress matches the values obtained on bulk samples, whereas the minimal value gives a hint of the smallest grain size. We have also tested an exponential distribution, because the Weibull exponent was found close to 1, but the agreement is less satisfactory.

Panels a and b in Figure 9 show the Mg substitution and grain size effects on the $Co_{0.6}Mg_{0.4}MoO_4$ compound behavior versus pressure, respectively. Both parameters led to the same tendencies than those observed in the isostatical pressure mode. Also in the uniaxial mode, the transition pressures are increased versus the grain size decrease and Co for Mg susbtitution. Comparing the P50 transition pressures, the Mg substitution shifted

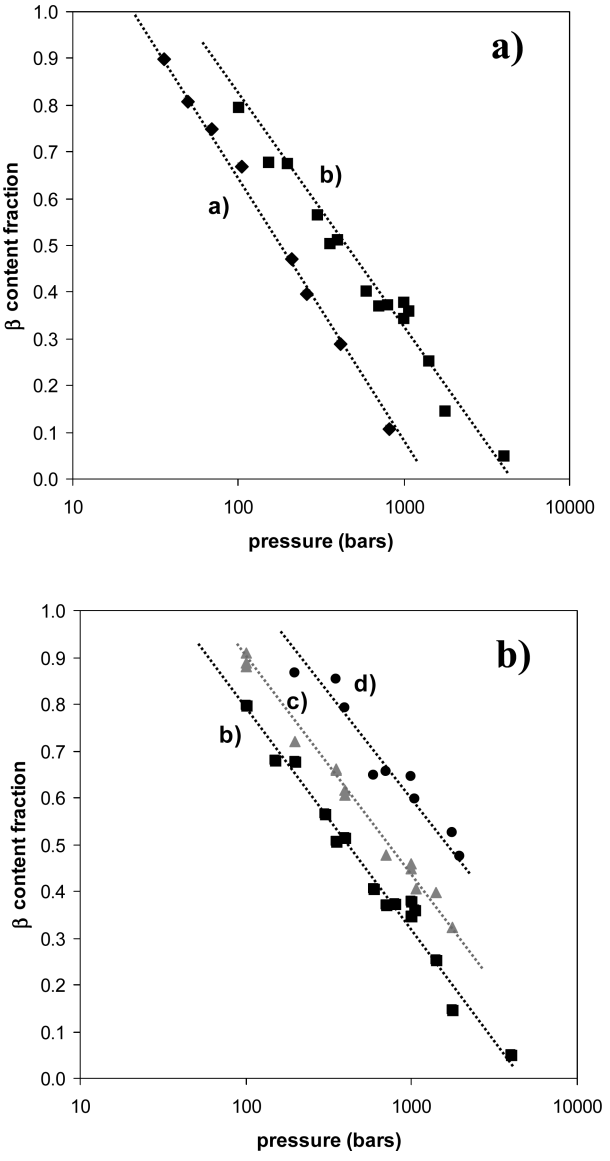

Figure 9. (a) β-form content versus applied pressure using uniaxial mode for (a) $CoMoO_4$ and (b) $Co_{0.6}Mg_{0.4}MoO_4$ compound. (b) β-form content versus applied pressure using uniaxial mode for (a) fresh $CoMoO_4$ and $CoMoO_4$ obtained after grinding for (b) 30 and (c) 120 min.

the transition form 200 bar (for $CoMoO_4$) to about 500 bar ($Co_{0.6}Mg_{0.4}MoO_4$), i.e., in quite the same amplitudes than in the isostatitical mode. The P50 transition pressures increase from the

fresh oxide (via the 30′ ground compound) to the 120′ ground compound from 200 bar (via 400 bar) to about 1500 bar. The grain size effect varied also roughly in the same proportion in both pressure application modes.

CONCLUSION

New piezochromic oxides were tested using two different pressure application modes: an isostatical mode through a liquid media and a uniaxial mode on powder pellets.

Similar influences of the oxide composition and grain size on the transition pressures were observed: the transition pressures increase while the grain size decrease and while Co was substituted for Mg in similar proportions whatever the application pressure mode. Two intrinsic key parameters allowing the transition pressure control were brought to the fore. In a applicative point of view, the new materials studied here, which show a high optical contrast between low and high pressure forms, can be used as pressure easy-indicators/shock detectors allowing the characterization of a very large pressure range (from few bars to few kbars).

Comparing both pressure application modes, the transition pressure are 10 times lower for unixial pressure mode than with the isostatical one, and it was interpreted as a consequence of the small solid−solid contact areas through which pressure was conducted in the uniaxial pressure mode. Furthermore, the shape of the phase transformation as a function of the applied pressure curve radically moved from a S curve shape in isostatical mode to a logarythmic dependence in the uniaxial mode. From a fundamental point of view, this work opens new prospects in the study of the physical behavior of pressure fields induced in granular skeletons from an uniaxial constrain. For the uniaxial pressure application mode, an exponential distribution of the solid−solid contact areas inside the powder pellet was proposed to explain the logarythmic dependence of the phase transformation versus the applied strength.

AUTHOR INFORMATION

Corresponding Author

*E-mail: gaudon@icmcb-bordeaux.cnrs.fr.

ACKNOWLEDGMENT

The “Direction Générale de l’Equipement” (DGE) is acknowledged for financial support through the ARTIQ consortium.

REFERENCES

(1) Greenberg, C. B. *Thin Solid Films* **1994**, *251*, 81.

(2) Rodríguez, F.; Hernández, D.; Garcia-Jaca, J.; Ehrenberg, H.; Weitzel, H. *Phys. Rev. B: Condens. Matter* **2000**, *61*, 16497.

(3) Hernández, D.; Rodríguez, F.; Garcia-Jaca, J.; Ehrenberg, H.; Weitzel, H. *Physica B* **1999**, *265*, 181.

(4) Gaudon, M.; Deniard, P.; Demourgues, A.; Thiry, A. E.; Carbonera, C.; Le Nestour, A. L.; Largeteau, A.; Létard, J.-F.; Jobic, S. *Adv. Mater.* **2007**, *19*, 3517.

(5) Thiry, A. E.; Gaudon, M.; Payen, C.; Daro, N.; Létard, J.-F.; Gorsse, S.; Deniard, P.; Rocquefelte, X.; Demourgues, A.; Whangbo, M.-H.; Jobic, S. *Chem. Mater.* **2008**, *20*, 2075.

(6) Gaudon, M.; Thiry, A. E.; Largeteau, A.; Deniard, P.; Jobic, S.; Demourgues, A. *Inorg. Chem.* **2008**, *47*, 2404.

(7) Gaudon, M.; Carbonera, C.; Thiry, A. E.; Demourgues, A.; Deniard, P.; Payen, C.; Létard, J.-F.; Jobic, S. *Inorg. Chem.* **2007**, *46*, 10200.

(8) Gaudon, M.; Basly, B.; Fauque, Y.; Majimel, J.; Delville, M.-H. *Inorg. Chem.* **2009**, *48*, 2136.

(9) Gaudon, M.; Riml, C.; Turpain, A.; Labrugère, C.; Delville, M.-H. *Chem. Mater.* **2010**, *22*, 5905.

(10) Livage, C.; Hynaux, A.; Marrot, J.; Nogues, M.; Ferey, G. *J. Mater.Chem.* **2002**, *12*, 1423.

(11) Maione, A.; Devillers, M. *J. Solid State Chem.* **2004**, *177*, 2339.

(12) Rodriguez, J. A.; Chatuvedi, S.; Hanson, J. C.; Albornoz, A.; Brito, J. L. *J. Phys.Chem. B.* **1998**, *102*, 1347.

(13) Rodriguez, J. A.; Chatuvedi, S.; Hanson, J. C.; Maiti, A.; Brito, J. L. *J. Chem. Phys.* **2000**, *112*, 935.

(14) Robertson, L.; Gaudon, M.; Jobic, S.; Deniard, P.; Demourgues, A.; *Inorg. Chem.*, just-accepted, 2011, Manuscript ID: ic-2010−02079f.

(15) Ravikumar, R.V.S.S.N.; Chandrasekhar, A. V.; Ramamoorthy, L.; Reddy, B. J.; Reddy, Y. P.; Yamauchi, J.; Raoe, P. S. *J. Alloys Compd.* **2004**, *364*, 176.

(16) Sreedhar, B.; Sumalatha, C.; Yamada, H.; Kojima, K. *J. Non-Cryst. Solids* **1996**, *203*, 172.